Available online at www.sciencedirect.com

ScienceDirect

IFAC PapersOnline CONFERENCE PAPER ARCHIVE

IFAC PapersOnLine 51-15 (2018) 533–538

Nonparametric Identification of Time-Varying Human Joint Admittance ⋆

G. Cavallo, * M. van de Ruit, ** A. C. Schouten, ** J. W. van Wingerden, ** J. Lataire *

* *Dept. ELEC, Vrije Universiteit Brussel, Pleinlaan 2, 1050 Elsene, Belgium (e-mail: gaia.cavallo@vub.ac.be, john.lataire@vub.ac.be).*
** *Department of Biomechanical Engineering and Delft Center for Systems and Control, Delft University of Technology, Mekelweg 2, 2628DC Delft, The Netherlands (e-mail: m.l.vanderuit-1@tudelft.nl, a.c.schouten@tudelft.nl, j.w.vanwingerden@tudelft.nl)*

Abstract: In this study, a nonparametric method, developed in Lataire et al. (2012), is applied to the identification of linear time-varying human joint admittance. The aim of the method, denoted *Skirt Decomposition* method, is to reconstruct the time-varying system function. The main contribution of the paper is to evaluate the possibilities and limitations of the method for the identification of linear time-varying human joint admittance in simulation. The proposed method delivers an estimate of linear time-varying joint admittance from a single experimental trial, provided that a multisine is used as excitation signal. The trade-off between i) the frequency resolution of the dynamics, and ii) the allowable complexity of the time variation is explored.

Keywords: linear time-varying systems, system function, frequency domain, biomechanical system, non-parametric identification

1. INTRODUCTION

1.1 Identification of nonlinear human joint admittance

To perform daily tasks, the mechanical properties of the human joints continuously change. For instance, the joints of a leg are stiff during the stance phase of the gait cycle and slack during the swing phase. The dynamics of a human joint are represented by joint admittance, a measure which explains the relation between a torque disturbance applied to a joint and the resulting angular deflection (Hogan, 1984). Having a representation of the change of human joint admittance during motor activities is useful for different clinical purposes. A model of joint admittance during functional tasks can be employed to design powered prosthetic joints that adjust their properties by mimicking the dynamic behavior of human joints (Rouse et al., 2014). The incorporation of artificial components with variable admittance would improve the mobility of prosthetic devices, rendering motor tasks more natural and intuitive for the users (Rouse et al., 2014). Furthermore, models of joint admittance could be used for the understanding of movement disorders. Impairments such as dystonia and bradykinesia have been linked to abnormal control of the reflexive component of joint admittance (Johnson et al., 1991; Schouten et al., 2003) . The comparison of the behavior of impaired and unimpaired participants could provide a tool to understand the pathophysiology of movement disorders and to guide future therapy.

To build a model of human joint admittance, system identification (SI) methods can be used, starting from torque and position measurements obtained experimentally from human joints. Traditionally, a small amplitude input is applied around a fixed operating point, and joint admittance is identified using Linear Time-Invariant (LTI) methods (Kearney and Hunter, 1990; Mirbagheri et al., 2000; Van der Helm et al., 2002). The resulting model only provides a local approximation, since in reality joint admittance is nonlinear and varies with the operating point. In fact, there are several physiological and mechanical factors that constitute the operating point and affect joint admittance nonlinearly (Kearney et al., 1997). Joint angle, muscle activation level, and muscular fatigue are a few of the known examples. Changes in joint angle and activation level can cause a nonlinear change of the viscous and elastic properties of the tissues surrounding a joint. Joint angle can change the perceived joint inertia, the moment arm of the muscles and the level of the stretch of the tissues, while an increase in the activation level results in a higher level of muscular contraction. Finally, during prolonged muscular contractions, fatigue occurs, which reduces the maximal force that can be produced by a muscle. To obtain a model of the changes of joint admittance during functional tasks, the dependence on the operating point should be considered. Nevertheless, not all of the factors that affect joint admittance are known and measurable with sufficient accuracy (Ludvig et al., 2017) to describe the change of dynamics with respect to the operating point and employ Linear Parameter-Varying models. A strategy is to assume

⋆ This research was funded by the European Research Council under the European Union's Seventh Framework Programme (FP/2007-2013) ERC Grant Agreement n. 291339, the Research Foundation Flanders (FWO-Vlaanderen), and the Flemish Government (Methusalem Fund METH1).

10.1016/j.ifacol.2018.09.209

that the changes of joint admittance are caused by the passage of time, rather than by alterations of the operating point. Under this assumption, joint admittance can be represented by a Linear Time-Varying (LTV) model.

1.2 Problem definition and objective of the paper

In the literature there exist multiple methods that can be applied to the identification of LTV models and they can be broadly classified as *subspace* (Moaveni and Asgarieh, 2012; Verhaegen and Yu, 1995), *prediction error* (Bennett et al., 1992) and *nonparametric* methods (Louarroudi et al., 2012; Lataire et al., 2012; Ludvig and Perreault, 2012; Guarín et al., 2017). In the first group, the system is represented in state-space form and the fundamental dynamics are retrieved starting from Hankel matrices containing the measured data. In the second group, a predetermined parametric structure is fit to the system by minimization of a cost function. In the last group, the measured signals are used to retrieve the LTV frequency response function (FRF) or the impulse response function of a system. The LTV methods have been mostly applied to the identification of LTV physical systems such as wind turbines, compressors, and motion platforms (van Wingerden and Verhaegen, 2007), while the identification of LTV joint admittance has received less attention. The main challenges encountered in human experiments for the identification of LTV joint admittance are:

(i) The time variation of the operating point cannot be fully controlled (Ludvig et al., 2017).
(ii) The measured torque signals have a low signal-to-noise ratio (SNR) (around 18 dB in Vlaar et al. (2017)).
(iii) The observation time is limited.
(iv) The *a priori* knowledge on the system dynamics is limited.

A promising method for the identification of LTV joint admittance is the *Skirt Decomposition method* (Lataire et al., 2012). The method applies nonparametric identification procedures to retrieve the time-varying FRF of LTV systems. The main advantages are that the method does not require a parametrization of the system dynamics and that the method can deliver a reliable LTV estimate based on a single trial of recorded data. Nevertheless, the *Skirt Decomposition* method assumes that the time variation should be slow with respect to the system dynamics and smooth, and requires that the system is excited by a multisine signal, as explained further on. The method has been successfully applied to the identification of LTV electronic circuits. However, its application to electronic circuit did not encounter the challenges specific to human experiments mentioned above; transferring the identification procedures to human joint admittance could also present new challenges.

The contribution of this paper is to evaluate the possibilities and limitations of the *Skirt Decomposition* method on the identification of LTV human joint admittance. The method is applied to simulated data of a simplified LTV human joint admittance model. This is a crucial step towards the application to experimental human data. This study can provide insight on the effects that different experimental and identification parameters have on the identification of joint admittance.The *Skirt Decomposition* method will be briefly explained in Section 2 to provide the readers with the background required to understand the remainder of the paper and to present the employed notation. A more extensive explanation of the method can be found in Lataire et al. (2012).

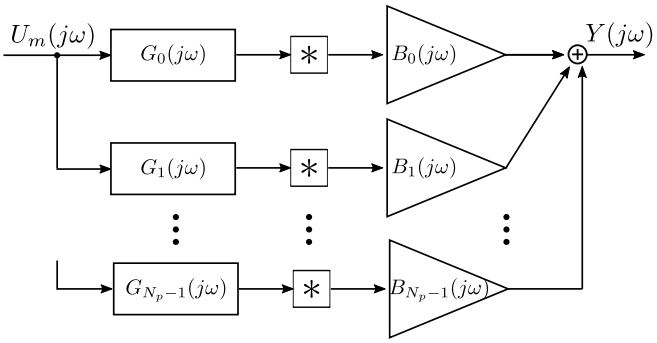

Fig. 1. Decomposition of the input $U_m(j\omega)$ into N_p branches, where $U_m(j\omega)$ is multiplied by an LTI component $G_p(j\omega)$, and the resulting signal is convolved with a basis function $B_p(j\omega)$. The sum of each branch determines the output $Y(j\omega)$.

2. SKIRT DECOMPOSITION METHOD

2.1 Modeling of LTV systems

The dynamics of an LTV system can be represented by its system function $G(j\omega, t)$: a 2-dimensional mapping which expresses how the frequency domain properties of the system evolve over time (Lataire et al., 2012). The system function can be expanded in a series consisting of LTI components $G_p(j\omega)$ multiplied by user-defined basis functions $b_p(t)$, $(p = 0, 1, .., N_p - 1)$, as:

$$G(j\omega, t) = \sum_{p=0}^{N_p-1} G_p(j\omega) b_p(t). \tag{1}$$

The time and frequency domain continuous-time response of an LTV system represented by (1), and excited by the signal $u(t)$, can be written respectively as:

$$\begin{aligned} y(t) &= \sum_{p=0}^{N_p-1} \mathcal{F}^{-1}\{U(j\omega)G_p(j\omega)\} b_p(t), \\ Y(j\omega) &= \sum_{p=0}^{N_p-1} \{U(j\omega)G_p(j\omega)\} * B_p(j\omega), \end{aligned} \tag{2}$$

where $\mathcal{F}^{-1}$ is the inverse Fourier operator, $U(j\omega)$ is the excitation signal in the Fourier domain, "$*$" is the convolution operator and $B_p(j\omega)$ is the Fourier transform of $b_p(t)$. Each term in (2), depicted by a branch in Figure 1, is composed of the convolution of an LTI response $\{U(j\omega)G_p(j\omega)\}$ and a basis function $B_p(j\omega)$.

2.2 Main identification steps

The *Skirt Decomposition* method is a nonparametric SI approach which fits the spectrum of predetermined basis functions onto the output spectrum of an LTV system, with the aim of reconstructing the LTV system function $G(j\omega, t)$. The method makes the following assumptions:

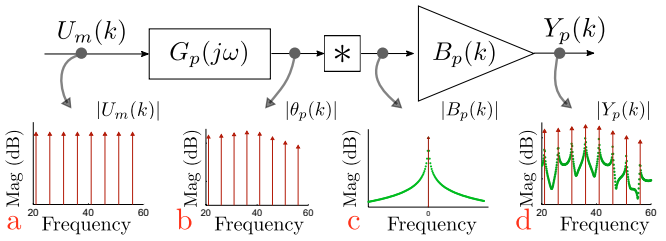

Fig. 2. Visualization of the steps representing (2) for a single branch and Discrete Fourier Transform of the signals (Adapted from Lataire et al. (2012)).

Assumption 1. The time variation of the target system is smooth and slow compared to the system dynamics. Consequently, the time variation can be represented in the frequency domain by functions with power concentrated at low frequencies, typically shaped as *"skirts"*.

Assumption 2. The input of the system is a multisine signal, defined as:

$$u_m(t) = \sum_{k_e \in \mathbb{K}_e} A(k_e)\cos(\omega_{k_e} t + \varphi_{k_e}), \tag{3}$$

where $\mathbb{K}_e$ is the set of the excited frequency bins considered, containing N_e elements, $\omega_{k_e} = 2\pi k_e/T$ are the excited angular frequencies of the sinusoids, with T equal to the length of the signal in time, and φ_{k_e} are the phases, randomly distributed between $-\pi$ and π.

If a multisine signal (Figure 2.a) is applied to an LTV system, each term of (2) is determined by the convolution of an LTI response with power at the excitation frequencies only (Figure 2.b) and a skirt (Figure 2.c). The result is the repetition of skirts around each excitation frequency (Figure 2.d). By summing each term of (2), the shape of the amplitude output spectrum presents the repetition of peaks and valleys; the portion of the spectrum between two valleys is composed of the sum of N_p skirts. For a sparse multisine, the contribution of each skirt in the output spectrum can be discerned by using linear least-squares regression on the measured output spectrum and on the predetermined basis functions. To reduce the computational time, the following assumption is made:

Assumption 3. The power of the output at each non-excited frequency is mainly determined by the skirts centered around the three closest excitation frequencies. The contribution of the neglected skirts can be modeled as a polynomial of order N_{tr}, denoted P_y. P_y also captures the transient dynamics.

The expression of the output Discrete Fourier Transform (DFT) spectrum is:

$$Y(k) = \frac{1}{N}\sum_{k'_e \in \mathbb{K}'_e}\sum_{p=0}^{N_p-1}\{U_m(k'_e)G_p(j\omega_{k'_e})\}B_p(k-k'_e)+P_y(k), \tag{4}$$

where $Y(k)$, $U_m(k)$ and $B_p(k)$ are respectively the DFTs of $y(t)$, $u_m(t)$ and $b_p(t)$, while $\mathbb{K}'_e$ is a subset of $\mathbb{K}_e$ and contains the bins corresponding to the three excitation frequencies closest to the bin k. Starting from (4), a linear least-squares regression is performed N_e times and $G_p(j\omega_{k_e})$ and $P_y(k)$ are computed. The system function is reconstructed using (1); however, since G_p is only expressed for $k_e \in \mathbb{K}_e$, the system function is computed at the excitation frequencies only.

3. SIMULATION STUDY

3.1 Simulink model

A mass-spring-damper model with the stiffness varying in time was implemented in Simulink (The Mathworks inc.) to represent the LTV intrinsic human joint admittance. In LTI conditions, it is common practice to represent intrinsic joint admittance with a linear mass-spring-damper model (De Vlugt et al., 2002; Schouten et al., 2008). The time variation was introduced by imposing a change of stiffness following the structure used in Ludvig and Perreault (2012). The dynamics of the model are represented by:

$$I_c\frac{d^2\phi(t)}{dt^2} = [\tau(t) - B_c\frac{d\phi(t)}{dt} - K(t)\phi(t)]. \tag{5}$$

In (5), the imposed torque $\tau(t)$ and the angular position $\phi(t)$ are the input and output of the system, respectively. The scalars I_c and B_c are the inertia and viscosity constants, while the function $K(t)$ represents the time-varying stiffness. For a fixed time instant t_i, the frozen transfer function representing the system in the Laplace domain is:

$$\frac{\Phi(s)}{\mathcal{T}(s)} = \frac{1}{I_c s^2 + B_c s + K(t_i)}, \tag{6}$$

with s the Laplace variable, $\mathcal{T}(s)$ and $\Phi(s)$ the input and the output in the Laplace domain.

3.2 Simulations

The input of the simulation model is composed of the repetition of 20 identical multisine signals with a period T_m of 10 s each. Zero-mean white noise, designed to result in an output SNR around 22 dB, was added to the output of the simulation. The frequency resolution of the output spectrum, depending upon the overall simulation time T and defining the distance between frequency bins, is equal to $1/T = 0.005$ Hz. However, since 20 periods of the multisine are repeated within the simulation time, the set $\mathbb{K}_e$ only contains integer multiples of 20. This is a trick to introduce unexcited frequencies in between each pair of excited frequencies.

For each combination of the tested model parameters, the simulation was run twice, each time with a different realization of the input signal and output noise, yet with the same set $\mathbb{K}_e$. Therefore, for each tested condition, two data sets were obtained: one for estimation and one for validation. The estimation data set was used to estimate a model of the system. The input from the validation data set was applied to the model to obtain an estimate of the output.

3.3 Model and identification parameters

Three case studies (*CS1*, *CS2* and *CS3*) with a different time-varying stiffness were considered (Figure 3). In *CS1* the stiffness varied proportionally with time, in *CS2* the stiffness followed the reciprocal of a linear function (hyperbola), and in *CS3* the stiffness varied sinusoidally. In all the three cases the stiffness ranged between

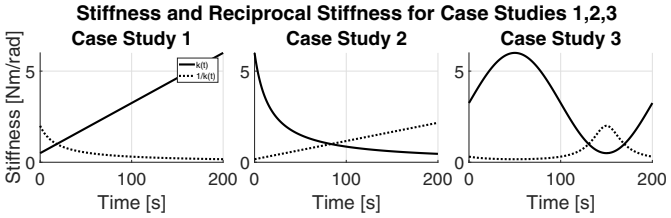

Fig. 3. Time-varying stiffness for *CS 1, 2* and *3*. Continuous black line: stiffness. Dotted black line: reciprocal of the stiffness.

0.4 Nm/rad and 6 Nm/rad. The inertia was set constant to 0.02 Nms^2/rad and the damping to 0.05 Nms/rad. These values are representative of the dynamics of the wrist (Schouten et al., 2008). The basis functions used are Legendre polynomials, shifted and scaled in time. The polynomials are defined as in Lataire et al. (2012), where it is shown that they result in a good numerical conditioning. The sampling frequency was 200 Hz. Finally, the simulation time was fixed at 200 s, to emulate the constraints on the observation time of a realistic experiment on humans. Two key design parameters were explored within the simulation and their combined effect on the performance of the *Skirt Decomposition* method was analyzed for the three case studies:

- Δf_{exc}, defining the distance, expressed in Hz, between each excitation frequency in the multisine signal. The design of Δf_{exc} has an influence on the frequency resolution of the system function, and on the overall number of the excitation frequencies. For each case study, the values tested are 0.2 Hz, 0.8 Hz and 1.4 Hz, corresponding to 40, 160 and 280 bins, respectively.
- N_p, representing the number of basis functions employed. The parameter influences the allowable complexity of the Skirts that can be distinguished in the output spectrum. For each case study, the value of N_p tested ranged from $N_p = 1$, corresponding to a single, constant basis function, to $N_p = 20$.

3.4 Performance analysis

The performance of the estimation is expressed in form of Variance Accounted For (VAF) and Root Mean Square Error (RMSE). The VAF was computed between the (sampled) noiseless validation output $y(t_k)$ and the (sampled) estimated output $\hat{y}(t_k)$, obtained from the validation input. The expression of the VAF is:

$$\text{VAF} = \max\left\{1 - \frac{\text{var}(y(t_k) - \hat{y}(t_k))}{\text{var}(y(t_k))}, 0\right\} \cdot 100\%. \qquad (7)$$

The RMSE was computed between the estimated resonance frequency and the true resonance frequency in time. The first was extracted from the estimated system function, and it is assumed to be equal to the frequencies corresponding to the highest magnitude of the system function. The true resonance frequency was computed as: $f_n(t) = \frac{1}{2\pi}\sqrt{\frac{K(t)}{I_c}}$. It is assumed that the frozen transfer function in (6) is a good approximation of the system function in (1).

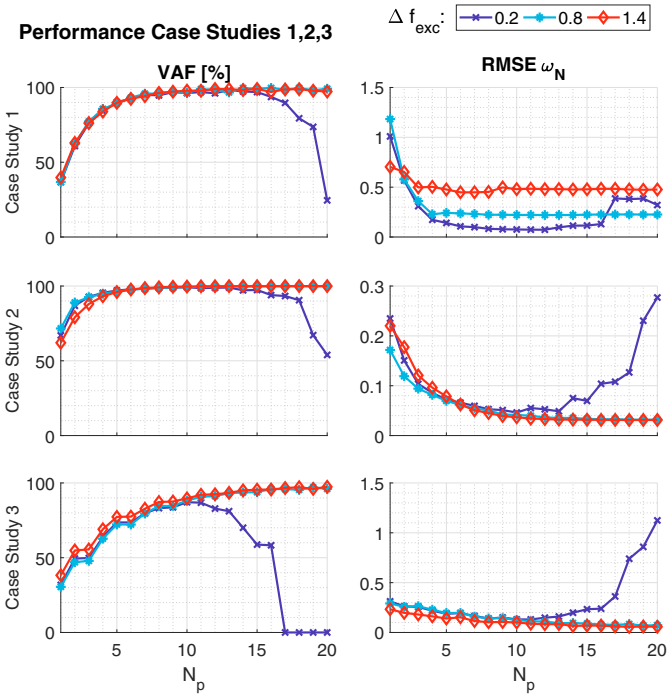

Fig. 4. Performance of the identified model on validation data sets for *CS 1, 2* and *3*, for N_p from 1 to 20 and $\Delta f_{\text{exc}} \in \{0.2, 0.8, 1.4\}$ Hz. Left column: The vertical axis represents the VAF of the estimated output. Right column: The vertical axis represents the RMSE of the estimated resonance frequency.

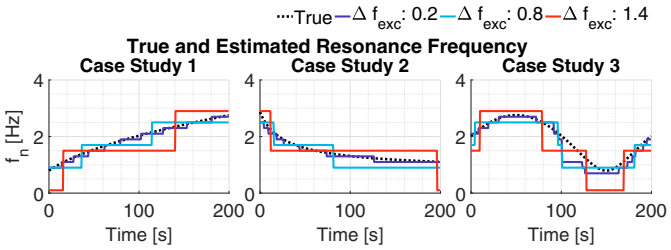

Fig. 5. Resonance frequency of *CS 1, 2* and *3* with N_p=10. Black line: resonance frequency of the system. Colored lines: resonance frequency retrieved for $\Delta f_{\text{exc}} \in \{0.2, 0.8, 1.4\}$ Hz.

3.5 Results

The VAF on the validation data sets and the RMSE of the estimated resonance frequency for the three case studies are depicted in Figure 4. In the first column, the VAF is shown for different combinations of Δf_{exc} and number of basis functions. For the three case studies, a common trend can be recognized: the VAF for $N_p = 1$ starts at a minimum value and it increases progressively with the order of the Legendre polynomial, reaching a maximum threshold around 100%. On the other hand, if a small Δf_{exc} (Δf_{exc}=0.2 Hz) is combined with a large N_p ($N_p \geq 14$) then the VAF decreases, dropping to 0%. A similar trend can be recognized in the second column, where the RMSE is plotted. The increment of N_p reduces the estimation error; nevertheless, if a large N_p is used with a small Δf_{exc}, the error increases.

Numerically, the structure of the varying stiffness has a strong effect on the performance. For $N_p = 1$, the VAF for *CS3* (sinusoidal stiffness) is around 30%, while the VAF for *CS2* (reciprocal stiffness) is about twice as large. For *CS1* (linear stiffness), the VAF has an intermediate value of around 40%. Furthermore, in *CS1* the maximum threshold of the VAF is reached for $N_p = 10$, in *CS2* for $N_p = 6$ and in *CS3* for $N_p = 16$. The value of Δf_{exc} has a visible effect on the RMSE in *CS1*: for Δf_{exc}=0.2 Hz the minimal RMSE is around 0.1 Hz, while for Δf_{exc}=1.4 Hz the minimum RMSE is about 0.5 Hz. Finally, it can be seen that for every case study, there exist at least one combination of N_p and Δf_{exc} that corresponds to a VAF higher than 90% and an RMSE lower than 0.1 Hz.

In Figure 5, the resonance frequency estimated from the three case studies for $N_p = 10$ is plotted against the resonance frequency extracted from the frozen transfer function. Whereas the system's resonance frequency (dotted line) presents a smooth behavior, the estimated resonance frequency (continuous lines) presents a step-like behavior. Δf_{exc} has an effect on how closely the step-like function matches the continuous smooth resonance frequency: a smaller Δf_{exc} corresponds to smaller steps and therefore to a closer fit.

4. DISCUSSION

4.1 Effects of design parameters on the estimation error

Number of basis functions N_p and distance between excitation frequencies Δf_{exc}. The performance generally increases with the number of basis functions N_p. With a higher N_p, more branches are used for the identification and the accuracy is improved. In other words, more skirts are employed to fit the output spectra, enhancing the degrees of freedom for the approximation and decreasing the bias error. However, a large N_p combined with a small Δf_{exc} result in low estimation accuracy. In fact, the skirts of higher order polynomials present a more complex and wide shape than lower order polynomials, whilst a small Δf_{exc} limits the bandwidth in which each skirt is expressed, resulting in the overlap of the contribution of neighboring skirts. Therefore, when a small Δf_{exc} is combined with a large N_p, the skirts become less distinguishable from each other, entailing a loss of precision (i.e. an increased variance) which is reflected in the identification results. The noise added to the output signal is an additional cause for the increased variance. When Δf_{exc} is small, there are not enough data points to distinguish the smooth contributions in the output spectrum from the random noise contribution, and discerning individual skirts becomes more challenging.

On the other hand, as seen in the right column of Figure 4 for *CS1*, a large Δf_{exc} increases the approximation error since the system function is computed at the excitation frequencies only. Therefore, the resolution of the system function and of the system properties, such as the resonance frequency, is limited by the value of Δf_{exc}. As confirmed in Figure 5, the resonance frequency retrieved from the estimated system function is only a quantized (discrete) approximation of the smooth resonance frequency of the system. The value of Δf_{exc} should be constrained to obtain a closer fit of the system function.

Complexity of the stiffness profile. Even though it is known that the time variation is introduced by the changes of stiffness in time, it is not straightforward to relate the complexity of the time variation to the changes of stiffness. Indeed, the effects of the latter are shaped by the system dynamics. An interesting result was the difference between *CS1* and *CS2* in the performance for low values of N_p in Figure 4. The complexity of *CS1*, where the stiffness profile was a linear function, resulted to be higher than in *CS2*, where the stiffness profile was a hyperbolic function. In fact, in *CS1* a higher number of basis functions than in *CS2* was required to reach high accuracy. The difference in performance is probably related to the complexity of the reciprocal stiffness, which determines the dynamics for ω=0 rad/s. As depicted in Figure 3, the reciprocal stiffness is more complex in *CS1* than in *CS2*. Therefore, in the system represented, the complexity of the time variation increases with the complexity of the reciprocal stiffness, as it could be expected from Equation (6).

4.2 Application of the Skirt Decomposition method to the identification of human joint admittance

The simulation study was performed to a condition with dynamics, bandwidth and frequency resolution representative of experiments for human joint admittance identification. For these conditions, intrinsically different from electronic circuits, three main factors with conflicting effects and requirements should be considered:

(i) The limited simulation time constrains the number of frequency bins available in the frequency band of interest.
(ii) A sufficient amount of bins between skirts should be guaranteed to be able to distinguish the individual effects of the skirts and to avoid an increase of the variance. The greater the complexity of the time variation and/or the noise level in the system, the further apart the excitation frequencies should be, if the frequency resolution is fixed.
(iii) Increasing the distance between excitation frequencies increases the quantization error in the approximation of the system function.

The excitation frequencies of the multisine input should be selected carefully as a trade-off value between the aforementioned factors, keeping into consideration the expected order of the time variation. For the condition tested, it was possible to find the right combination of N_p and Δf_{exc} to obtain a VAF with the noiseless output approaching 100% and a RMSE of the resonance frequency lower than 0.1 Hz for each case study.

To apply the method to a real experimental setup, it is important to consider the assumptions made by the *Skirt Decomposition* on the time variation. According to *Assumption 1*, the skirts in the output spectrum should have the power concentrated at the low frequencies. The Legendre polynomials are good candidates to approximate the slow time variation since their frequency spectrum is compatible with the assumption. Furthermore, Legendre polynomials have a high approximation power to fit time variations with different complexities. Indeed, for sufficiently high N_p, all the three case studies could be approximated with high accuracy. If the structure of the time

variation is known *a priori*, basis functions with a tailored frequency content could be used instead. In such a case, it would be possible to deal with systems with a faster time variation, since only a limited N_p is necessary to obtain a fit of the output spectrum, reducing the issues related to the overlapping of skirts explained in Section 4.1.1. The related cost is a loss of generality in the approximation of time variations with an arbitrary structure.

Using the results from the presented work, further research with promising results is being done on the application of the *Skirt Decomposition* method on human experimental data subject to a slow time variation. Furthermore, for specific conditions on human experiments, tailored basis functions are being considered to identify conditions with a faster time variation. Future work should be done to include the reflexive component of joint admittance in the simulated model, in order to assess the accuracy of the method for a wider set of experimental conditions.

5. CONCLUSIONS

The *Skirt Decomposition* method can be used to identify an LTV system with dynamics similar to those of human joint admittance. The application of the method requires a careful choice of parameters, especially when the complexity of the time variation is high. To allow the approximation of complex skirts, the number of basis functions should be large. Nevertheless, Δf_{exc} should be increased accordingly to avoid an increase of variance. However, a large Δf_{exc} results in a drop of the frequency resolution of the system function and an increase of the quantization error. Considering the simplified human-like model tested in this study, it was sufficient to employ 8 basis functions and excitation frequencies 0.8 Hz apart to accurately model the time-varying joint admittance.

REFERENCES

Bennett, D., Hollerbach, J., Xu, Y., and Hunter, I. (1992). Time-varying stiffness of human elbow joint during cyclic voluntary movement. *Experimental Brain Research*, 88(2), 433–442.

De Vlugt, E., Schouten, A.C., and Van Der Helm, F.C. (2002). Adaptation of reflexive feedback during arm posture to different environments. *Biological cybernetics*, 87(1), 10–26.

Guarín, D.L., Kearney, R.E., Guarín, D.L., and Kearney, R.E. (2017). Estimation of time-varying, intrinsic and reflex dynamic joint stiffness during movement. application to the ankle joint. *Frontiers in computational neuroscience*, 11, 51.

Hogan, N. (1984). Adaptive control of mechanical impedance by coactivation of antagonist muscles. *IEEE Transactions on Automatic Control*, 29(8), 681–690.

Johnson, M., Kipnis, A., Lee, M., Loewenson, R., and Ebner, T. (1991). Modulation of the stretch reflex during volitional sinusoidal tracking in parkinson's disease. *Brain*, 114(1), 443–460.

Kearney, R.E. and Hunter, I.W. (1990). System identification of human joint dynamics. *Critical reviews in biomedical engineering*, 18(1), 55–87.

Kearney, R.E., Stein, R.B., and Parameswaran, L. (1997). Identification of intrinsic and reflex contributions to human ankle stiffness dynamics. *IEEE Transactions on Biomedical Engineering*, 44(6), 493–504.

Lataire, J., Pintelon, R., and Louarroudi, E. (2012). Nonparametric estimate of the system function of a time-varying system. *Automatica*, 48(4), 666–672.

Louarroudi, E., Pintelon, R., and Lataire, J. (2012). Nonparametric tracking of the time-varying dynamics of weakly nonlinear periodically time-varying systems using periodic inputs. *IEEE Transactions on Instrumentation and Measurement*, 61(5), 1384–1394.

Ludvig, D. and Perreault, E.J. (2012). System identification of physiological systems using short data segments. *IEEE Transactions on Biomedical Engineering*, 59(12), 3541–3549.

Ludvig, D., Plocharski, M., Plocharski, P., and Perreault, E.J. (2017). Mechanisms contributing to reduced knee stiffness during movement. *Experimental brain research*, 235(10), 2959–2970.

Mirbagheri, M., Barbeau, H., and Kearney, R. (2000). Intrinsic and reflex contributions to human ankle stiffness: variation with activation level and position. *Experimental Brain Research*, 135(4), 423–436.

Moaveni, B. and Asgarieh, E. (2012). Deterministic-stochastic subspace identification method for identification of nonlinear structures as time-varying linear systems. *Mechanical Systems and Signal Processing*, 31, 40–55.

Rouse, E.J., Hargrove, L.J., Perreault, E.J., and Kuiken, T.A. (2014). Estimation of human ankle impedance during the stance phase of walking. *IEEE Transactions on Neural Systems and Rehabilitation Engineering*, 22(4), 870–878.

Schouten, A., Van de Beek, W., Van Hilten, J., and Van der Helm, F. (2003). Proprioceptive reflexes in patients with reflex sympathetic dystrophy. *Experimental brain research*, 151(1), 1–8.

Schouten, A.C., De Vlugt, E., Van Hilten, J., and Van Der Helm, F.C. (2008). Quantifying proprioceptive reflexes during position control of the human arm. *IEEE Transactions on Biomedical Engineering*, 55(1), 311–321.

Van der Helm, F.C., Schouten, A.C., de Vlugt, E., and Brouwn, G.G. (2002). Identification of intrinsic and reflexive components of human arm dynamics during postural control. *Journal of neuroscience methods*, 119(1), 1–14.

van Wingerden, J.W. and Verhaegen, M. (2007). Subspace identification of bilinear systems using a dedicated input sequence. In *Proceedings of Decision and Control IEEE Conference*, 4962–4967.

Verhaegen, M. and Yu, X. (1995). A class of subspace model identification algorithms to identify periodically and arbitrarily time-varying systems. *Automatica*, 31(2), 201–216.

Vlaar, M.P., Solis-Escalante, T., Vardy, A.N., Van Der Helm, F.C., and Schouten, A.C. (2017). Quantifying nonlinear contributions to cortical responses evoked by continuous wrist manipulation. *IEEE transactions on neural systems and rehabilitation engineering*, 25(5), 481–491.